

Communication

# Theoretical Investigation of a Coumarin Fluorescent Probe for Distinguishing the Detection of Small-Molecule Biothiols

Yue Deng, He Huang, Jian Feng, Yongjin Peng \*  and Yuling Liu \*

College of Modern Industry of Health Management, Jinzhou Medical University, Jinzhou 121001, China

\* Correspondence: hunterpyj2016@163.com (Y.P.); jzmulyl@163.com (Y.L.)

**Abstract:** Monitoring the level of biothiols in organisms would be beneficial for health inspections. Recently, 3-(2'-nitro vinyl)-4-phenylselenyl coumarin as a fluorescent probe for distinguishing the detection of the small-molecule biothiols cysteine/homocysteine (Cys/Hcy) and glutathione (GSH) was developed. By introducing 4-phenylselenium as the active site, the probe CouSeNO<sub>2</sub>/CouSNO<sub>2</sub> was capable of detecting Cys/Hcy and GSH in dual fluorescence channels. Theoretical insights into the fluorescence sensing mechanism of the probe were provided in this work. The details of the electron excitation process in the probe and sensing products under optical excitation and the fluorescent character were analyzed using the quantum mechanical method. All these theoretical results would provide insight and pave the way for the molecular design of fluorescent probes for the detection of biothiols.

**Keywords:** fluorescent probe; biothiols; theoretical investigation; electron excitation

## 1. Introduction

Biothiols are involved in many processes of transfer and detoxification, including cell growth, redox, and so on. Small molecular biothiols, including cysteine, homocysteine, and glutathione (Cys, Hcy, and GSH, respectively), are important sulfur compounds that could protect parts of the body due to their reducibility [1–3]. Biothiols with structural differences would lead to different functions; meanwhile, the biothiols are related to each other. Cys is involved in the process of enzyme catalysis, detoxification, and protein synthesis. Hcy is a regulatory intermediate in the Met cycle and the precursors of Cys and methionine. GSH has a role in maintaining redox homeostasis in biological systems.

The concentration of biological biothiols will deviate from normal values under the influence of adverse factors and directly affect their functions. In this situation, diseases such as growth retardation, cardiovascular disease, liver damage, and rheumatism, etc., could be caused. Therefore, monitoring the level of biothiols in organisms would be beneficial for health inspections. Nowadays, the methods of detecting biothiols are diversified and gradually improved. Yet, different detection methods have their own advantages and drawbacks [2,4–10].

At present, the main methods for the detection and analysis of active sulfur species (RSS) include the high-performance liquid chromatography (HPLC) analytical method, the colorimetric method, mass spectrometry, electrochemical analysis, capillary electrophoresis, and fluorescence analysis [11–16].

According to the comparative analysis, the detection results of high-performance liquid chromatography and mass spectrometry are relatively stable and sensitive but necessitate complicated sample operations and expensive equipment. The capillary electrophoresis detection method is economical and rapid, but has slightly inferior sensitivity. Colorimetry is easy to use but usually produces a relatively big error. Although the electrochemical analysis method has the advantages of convenience and high sensitivity, it is relatively weak in terms of selectivity. In contrast, fluorescent probes have been successfully



**Citation:** Deng, Y.; Huang, H.; Feng, J.; Peng, Y.; Liu, Y. Theoretical Investigation of a Coumarin Fluorescent Probe for Distinguishing the Detection of Small-Molecule Biothiols. *Molecules* **2024**, *29*, 554. <https://doi.org/10.3390/molecules29030554>

Academic Editor: Evangelos Miliordos

Received: 7 December 2023

Revised: 6 January 2024

Accepted: 10 January 2024

Published: 23 January 2024



**Copyright:** © 2024 by the authors. Licensee MDPI, Basel, Switzerland. This article is an open access article distributed under the terms and conditions of the Creative Commons Attribution (CC BY) license (<https://creativecommons.org/licenses/by/4.0/>).

applied to many detection fields due to their advantages of high sensitivity, low background interference, high selectivity, and good biocompatibility. Combined with focusing microscope instruments, fluorescent probes are applied to real-time and in situ imaging of biological cells and tissues without causing any damage, which provides a powerful analytical technique for disease diagnosis and is becoming a popular detection method in biological and medical fields.

In recent years, remarkable progress has been made in the construction of biothiol fluorescent probes [4,17–19]. Many reported fluorescent probes can be responded to biothiols in cells, tissues, and a variety of amino acids. However, due to the similar structure and reactivity of biothiols, most of the fluorescent probes reported so far cannot distinguish between the biothiols of Cys, Hcy, and GSH, which hinders the research of their roles in corresponding physiological and pathological processes [20,21].

Recently, Chen et al. developed 3-(2'-nitro vinyl)-4-phenylselenyl coumarin as a fluorescent probe for distinguishing between the detection of Cys/Hcy and GSH. By introducing 4-phenylselenium as the active site, the probe CouSeNO<sub>2</sub>/CouSNO<sub>2</sub> was capable of detecting Cys/Hcy and GSH in dual fluorescence channels [22]. For the biothiols, the first-step sensing reaction was experimentally proven to be the nucleophilic substitution of 4-phenylselenium with the thiol group. Furthermore, through two-channel fluorescent imaging, the probe CouSeNO<sub>2</sub>/CouSNO<sub>2</sub> had been successfully applied to sense the exogenous and endogenous biothiols in living cells. Except for the Michael addition as a usual sensing reaction in reported nitroolefin fluorescent probes, the nucleophilic substitution of 4-phenylselenium in the probe CouSeNO<sub>2</sub>/CouSNO<sub>2</sub> with the thiol group of a biothiol as the first-step sensing reaction not only accelerated the reaction to biothiols but also realized the distinction between Cys/Hcy and GSH in dual fluorescence channels. Compared with the experimental results, the theoretical research on the electronic structure, reaction sites, sensing mechanism, and fluorescent properties of the probe CouSeNO<sub>2</sub>/CouSNO<sub>2</sub> in this work could provide insights and pave the way for the molecular design of fluorescent probes for the detection of biothiols.

## 2. Results and Discussion

The stable molecular structures of the probes CouClNO<sub>2</sub>, CouSNO<sub>2</sub>, and CouSeNO<sub>2</sub> are shown in Figure 1a–c. Due to no apparent spectral response with biothiols, the probe CouClNO<sub>2</sub> was only presented for structural comparison here but not for consideration in the following theoretical research.

From the surface map of average local ionization energy (ALIE) [23] on three probes in Figure 1d–f, it could be deduced that the C=C bond in CouClNO<sub>2</sub> is the potential electrophilic reaction site (with an ALIE value of 0.33 a.u.); otherwise, the S(Se) atom and C=C bond in the CouSNO<sub>2</sub> and CouSeNO<sub>2</sub> probes are the potential electrophilic reaction sites (with the ALIE values of 0.32 a.u. and 0.30 a.u. for the S and Se atoms in the CouSNO<sub>2</sub> and CouSeNO<sub>2</sub> probes, respectively).

Fukui function and dual descriptor, known as the important concepts in density functional reactivity theory, which was initially developed by Parr, are very popular methods for predicting reaction sites defined under the conceptual density functional theory framework [24–26]. The dual descriptors of the CouClNO<sub>2</sub>, CouSNO<sub>2</sub>, and CouSeNO<sub>2</sub> probes were obtained through Multiwfn 3.8(dev) analysis based on the ORCA output results and are illustrated in Figure 1g–i. The S and Se atoms in the CouSNO<sub>2</sub> and CouSeNO<sub>2</sub> probes (indicated by the red circle in Figure 1h,i) were indicated to be the potential electrophilic reaction sites with biothiols, which were in agreement with the corresponding experimental results [22]. The lower ALIE value of the Se atom compared to the S atom indicated the higher sensitivity of the CouSeNO<sub>2</sub> probe to biothiols than the CouSNO<sub>2</sub> probe, which was also testified within the experiment work.

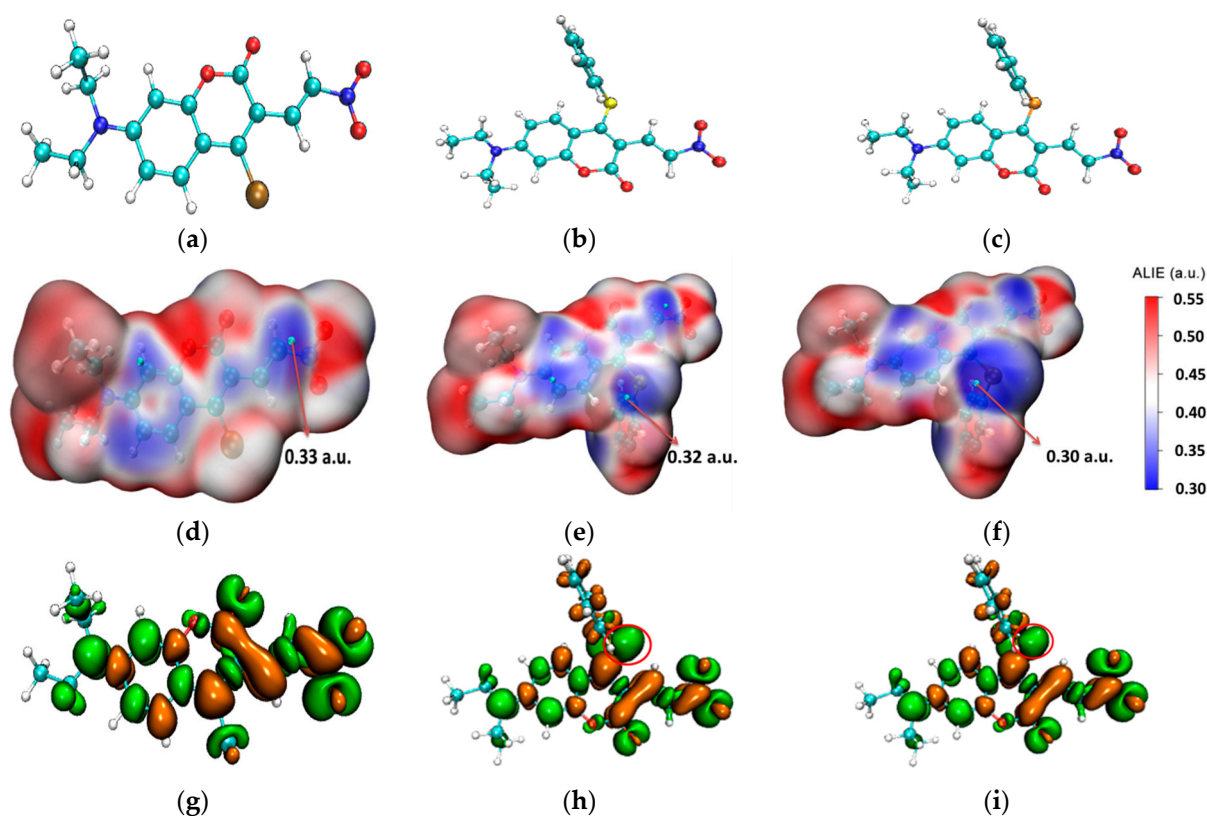


**Figure 1.** (a–c) The stable molecular structures of the CouCINO<sub>2</sub>, CouSNO<sub>2</sub>, and CouSeNO<sub>2</sub> probes; (d–f) the surface map of ALIE on the CouCINO<sub>2</sub>, CouSNO<sub>2</sub>, and CouSeNO<sub>2</sub> probes; and (g–i) the dual descriptors of the CouCINO<sub>2</sub>, CouSNO<sub>2</sub>, and CouSeNO<sub>2</sub> probes. (the red circle indicate S and Se atom in the CouSNO<sub>2</sub> and CouSeNO<sub>2</sub> probes respectively).

From the 2D plots of dual descriptors on the main molecular planes of the CouSNO<sub>2</sub> and CouSeNO<sub>2</sub> probes, as shown in Figure 2a,b, the dual descriptor absolute values of the S and Se atoms are obviously larger than the values at other places within the probe molecule. This result indicated that a substitution reaction would likely occur within the S and Se atoms when the CouSNO<sub>2</sub> and CouSNO<sub>2</sub> probes encountered the biothiols. The 2D localized orbital locator (lol) on the molecular planes of the CouSNO<sub>2</sub> and CouSeNO<sub>2</sub> probes, as shown in Figure 2c,d, also indicated that the S and Se atoms in the probe molecules were potential reaction sites. The sensing mechanism of CouSeNO<sub>2</sub> towards biothiols is shown in Scheme 1.

The most stable geometric structures of the ground state S<sub>0</sub> and first excited state S<sub>1</sub> of the CouSNO<sub>2</sub> and CouSeNO<sub>2</sub> probes are shown in Figure 3. It indicated a similar difference between the S<sub>0</sub> and S<sub>1</sub> structures of the CouSNO<sub>2</sub> and CouSeNO<sub>2</sub> probes, in which the benzene ring showed an obvious flip from the ground state to the first excited state. The dihedral angle,  $\alpha$ , between the benzene ring and the main molecular plane of the CouSNO<sub>2</sub> probe varied from 59° to 108° when the molecule was excited from S<sub>0</sub> to S<sub>1</sub>; this change in  $\alpha$  was from 56° to 108° in the CouSeNO<sub>2</sub> probe. This large structural difference between S<sub>0</sub> and S<sub>1</sub> within the CouSNO<sub>2</sub> and CouSeNO<sub>2</sub> probes would lead to large reorganization energy and Huang–Rhys factors [27,28] for some normal vibration modes, as shown in Figure 4 (CouSNO<sub>2</sub> was only shown for clarity consideration). It could be seen that the vibration mode with large Huang–Rhys factors were just corresponding with the swing of the benzene ring in the probe molecule. The reorganization energy and Huang–Rhys factors between S<sub>0</sub> and S<sub>1</sub> of the CouSNO<sub>2</sub> and CouSeNO<sub>2</sub> probes were calculated through the Dushin program [29].

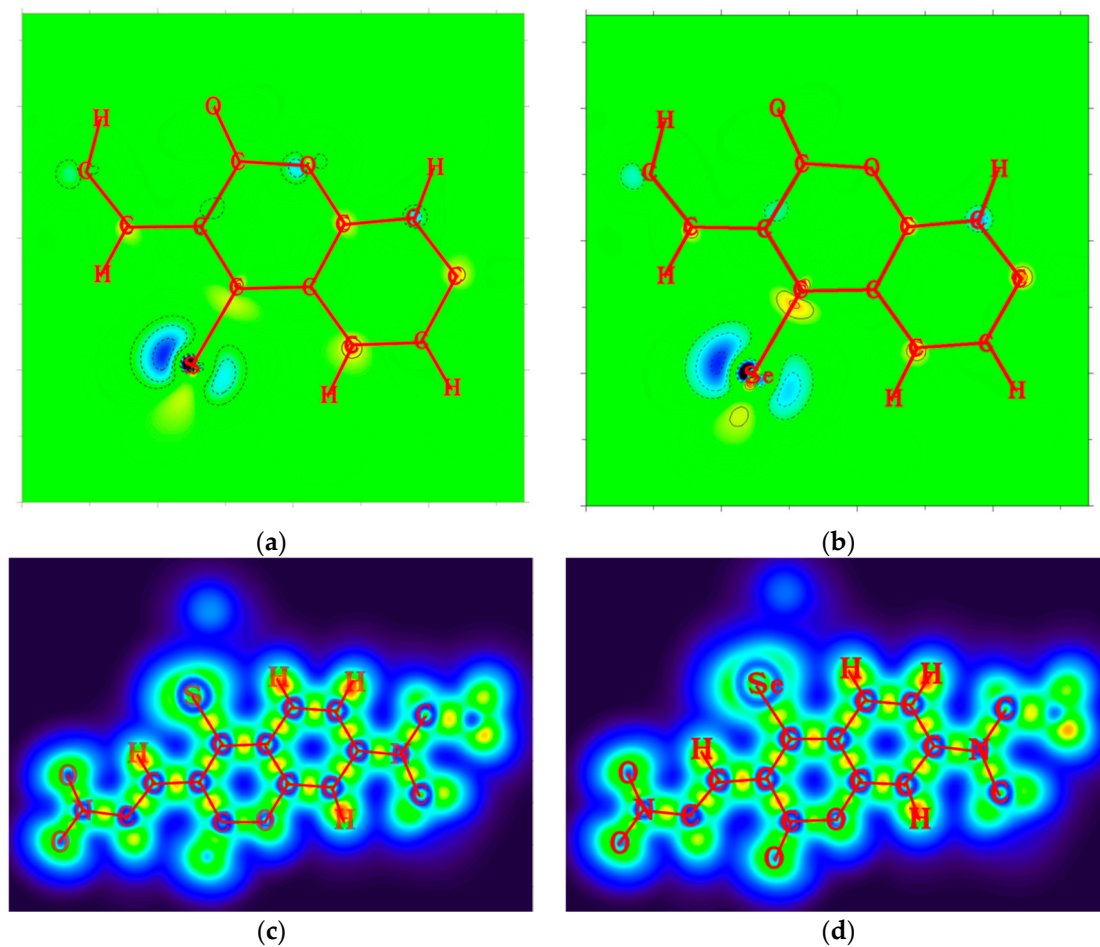
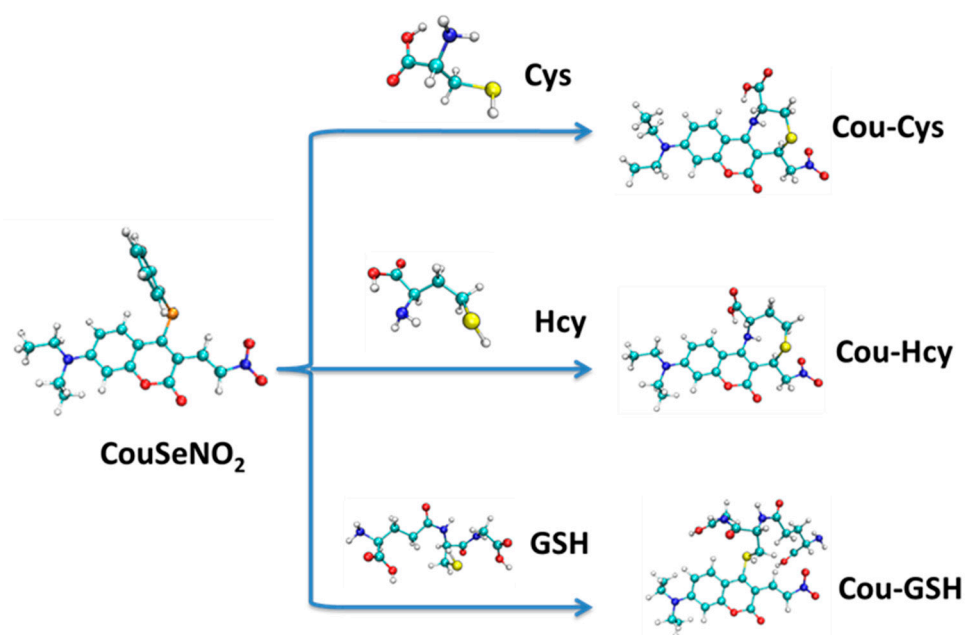


**Figure 2.** (a,b) Two-dimensional plots of dual descriptors on the molecular planes of the CouSNO<sub>2</sub> and CouSeNO<sub>2</sub> probes; (c,d) 2D IOL on the molecular planes of the CouSNO<sub>2</sub> and CouSeNO<sub>2</sub> probes.



**Scheme 1.** The sensing mechanism of CouSeNO<sub>2</sub> towards biothiols.

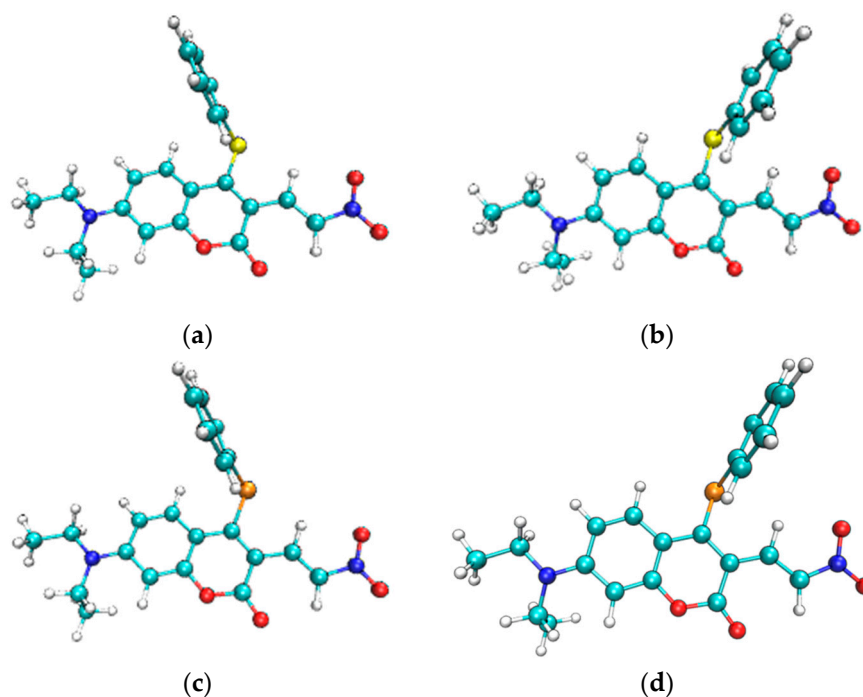


**Figure 3.** (a,b) Geometric structures of the  $S_0$  and  $S_1$  of the CouSNO<sub>2</sub> probe; and (c,d) geometric structures of the  $S_0$  and  $S_1$  of the CouSeNO<sub>2</sub> probe.

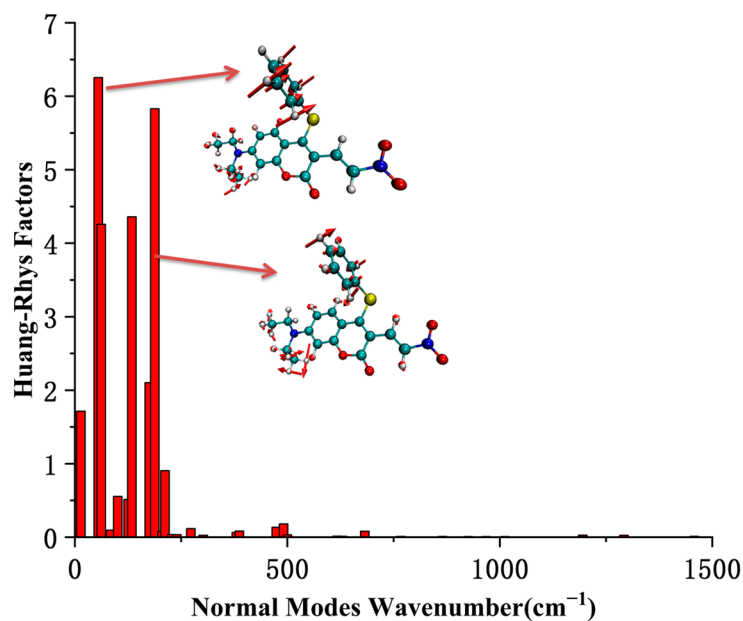


**Figure 4.** The Huang–Rhys factors of the CouSNO<sub>2</sub> probe.

To illustrate the electron excitation process from  $S_0$  to  $S_1$  within the CouSNO<sub>2</sub> and CouSeNO<sub>2</sub> probes, the hole–electron (brown and green colors, respectively, in Figure 5) analyses were performed based on the TDDFT results. It could be informed that the electron was mainly excited from the benzene ring part to the main planar part of the probes. The excitation energy from  $S_0$  to  $S_1$  in CouSeNO<sub>2</sub> (3.940 eV) was a little larger than that in CouSNO<sub>2</sub> (3.917 eV).

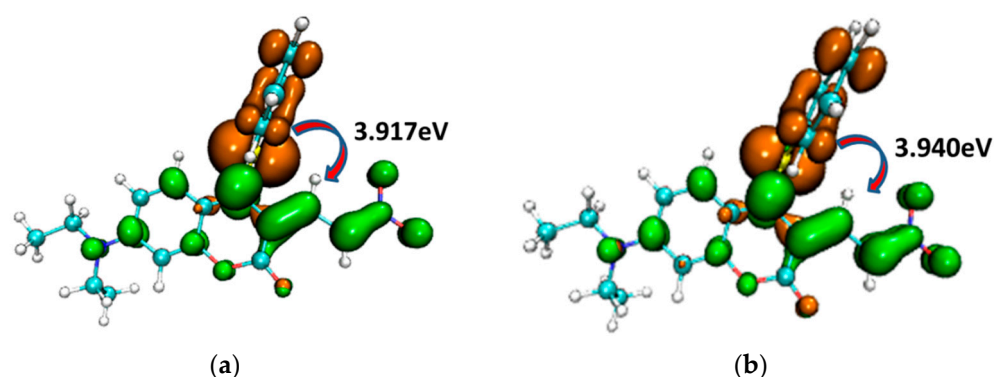


**Figure 5.** Hole–electron (brown and green colors, respectively) analysis for the electron excitation process from  $S_0$  to  $S_1$  within the (a) CouSNO<sub>2</sub> and (b) CouSeNO<sub>2</sub> probes.

The simulated UV–Vis absorption spectrum of the CouSeNO<sub>2</sub> probe, as shown in Figure 6a, indicated that the absorption wavelength from  $S_0$  to  $S_1$  was about 473 nm, which was near the experimental value of 480 nm and testified to the reasonable choice of the functional and basis set for electron excitation calculation on this kind of organic molecular probe. After the reaction with Cys and Hcy, the absorption wavelengths from  $S_0$  to  $S_1$  of the sensing products Cou-Cys and Cou-Hcy were changed by a blue shift to be about 360 nm and 357 nm, respectively, which were consistent with the experimental results.

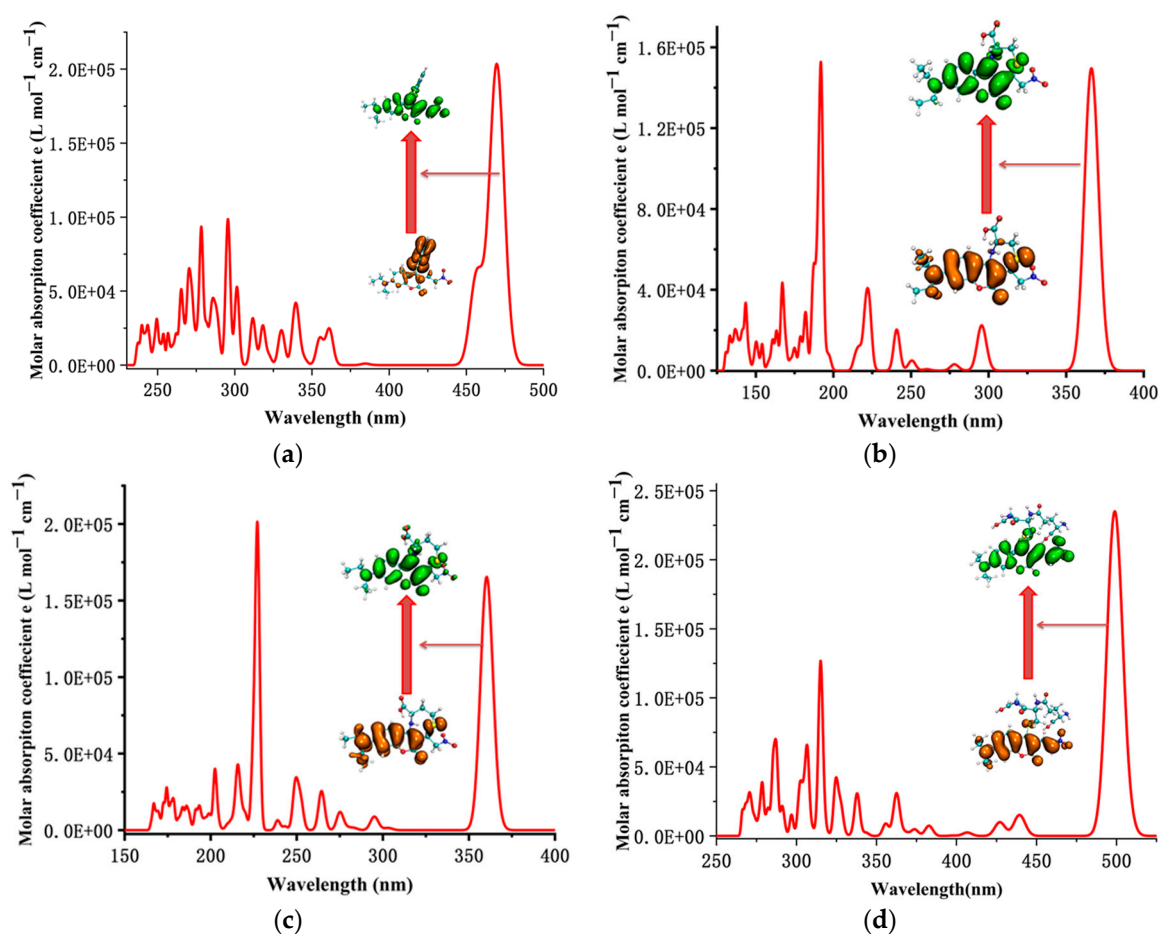


**Figure 6.** The simulated UV–Vis absorption spectrum of the probe and sensing products. (a) CouSeNO<sub>2</sub>. (b) Cou-Cys. (c) Cou-Hcy. (d) Cou-GSH.

Unlike the charge transfer characteristic of electron excitation in the process from  $S_0$  to  $S_1$  within the original CouSeNO<sub>2</sub> probe, it was shown the local excitation character for the electron excitation process from  $S_0$  to  $S_1$  within the sensing products Cou-Cys and Cou-Hcy, and this local excitation character led to a significant increase in the fluorescent intensity at about 460 nm and 451 nm, respectively, which were testified within both the theoretical and experimental results. A similar reaction between the CouSeNO<sub>2</sub> probe and GSH occurred, which also led to the variation in the UV–Vis absorption spectrum and fluorescent intensity of the sensing product Cou-GSH. Without the seven- or eight-membered ring like in sensing products Cou-Cys and Cou-Hcy, due to the Michael addition reaction of the thiol group to the unsaturated C=C double bond, there was a red shift within the UV–Vis absorption and fluorescent spectrum of sensing product Cou-GSH compared with the original probe CouSeNO<sub>2</sub>. The theoretical absorption and emission wavelength between  $S_0$  and  $S_1$  was about 500 nm and 550 nm, respectively, which were well agreed with the experimental values of 515 nm and 562 nm, respectively. The theoretical and experimental fluorescent-related absorption and emission wavelengths are summarized in Tables 1 and 2.

**Table 1.** The main electron excitation processes in the probe and sensing product molecule.

Probe/Sensing Product	Electronic Transition <sup>a</sup>	Excitation Energy Theoretical/Experimental (nm)	Oscillator Strength	Composition <sup>b</sup>	CI <sup>c</sup>
CouSeNO <sub>2</sub>	$S_0 \rightarrow S_1$	473/480	0.1063	H → L	0.6815
Cou-Cys	$S_0 \rightarrow S_1$	360/370	0.7921	H → L	0.6908
Cou-Hcy	$S_0 \rightarrow S_1$	357/365	0.8014	H → L	0.7014
Cou-GSH	$S_0 \rightarrow S_1$	500/515	0.7318	H → L	0.7219

<sup>a</sup> Only the excited states with an oscillator strength larger than 0.1 were considered. <sup>b</sup> H stands for HOMO and L stands for LUMO. <sup>c</sup> Coefficient of the wave function for each excitation was in absolute value.

**Table 2.** The main electron emission processes in the probe and sensing product molecule.

Probe/Sensing Product	Electronic Transition <sup>a</sup>	Emission Energy Theoretical/Experimental (nm)	Oscillator Strength	Composition <sup>b</sup>	CI <sup>c</sup>
CouSeNO <sub>2</sub>	$S_1 \rightarrow S_0$	498/N.A.	0.0245	H → L	0.6726
Cou-Cys	$S_1 \rightarrow S_0$	460/465	0.7146	H → L	0.7017
Cou-Hcy	$S_1 \rightarrow S_0$	451/457	0.7219	H → L	0.7102
Cou-GSH	$S_1 \rightarrow S_0$	550/562	0.6849	H → L	0.7115

<sup>a,b,c</sup> same indication as in Table 1.

To illustrate the electronic structures of the CouSeNO<sub>2</sub> probe and its sensing product with biothiols in more depth, the density of electronic states (DOSs) were calculated and are illustrated in Figure 7. The main orbital transition contribution to the electron excitation between  $S_0$  and  $S_1$  in the probes and sensing products was the highest occupied molecular orbit (HOMO) and the lowest unoccupied molecular orbit (LUMO), as shown in Tables 1 and 2. The fluorescence of the probes and sensing products were decided through the electron radiation process from  $S_1$  to  $S_0$ .

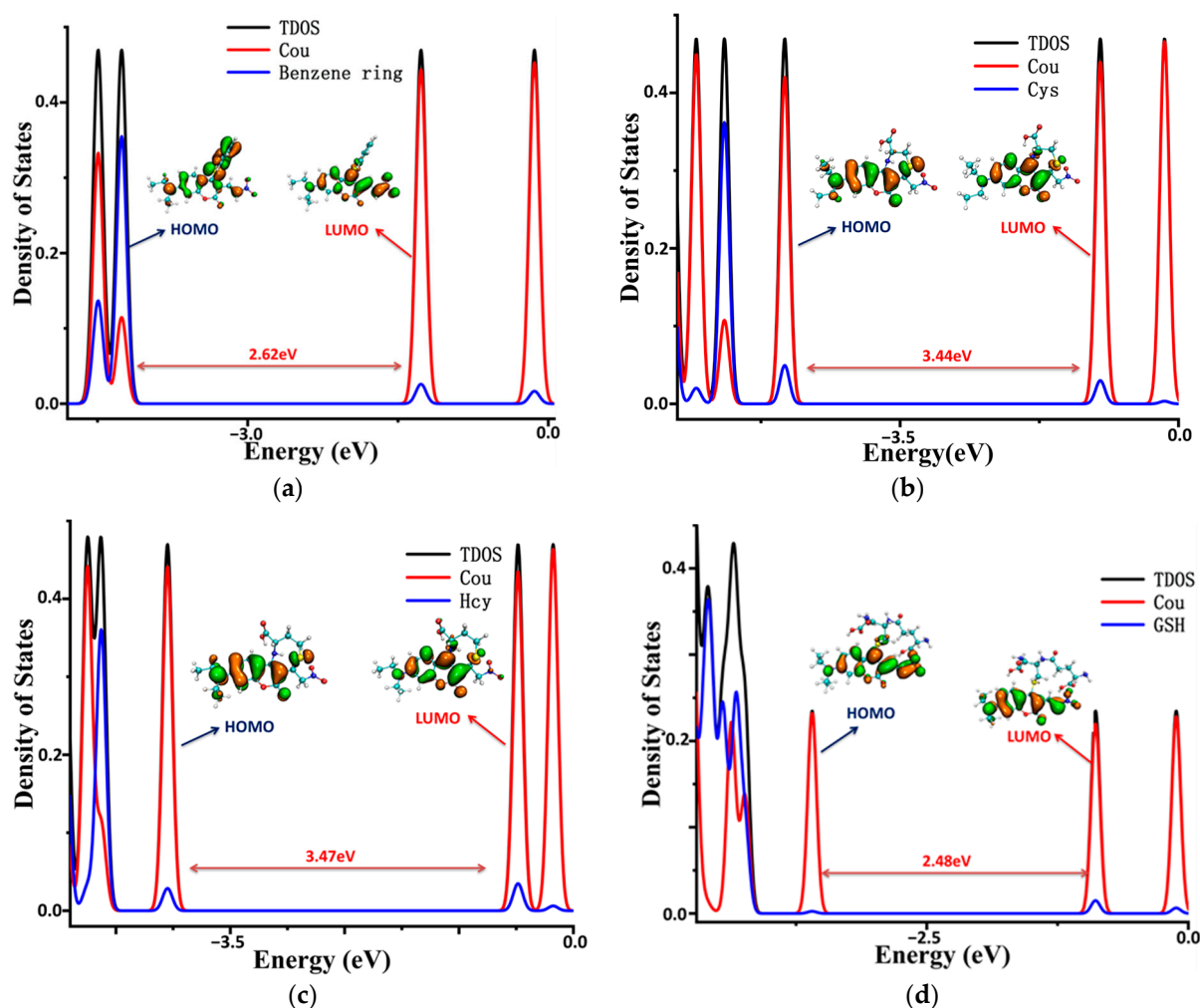


**Figure 7.** The density of the electronic states of the probe and sensing products. (a) CouSeNO<sub>2</sub>. (b) Cou-Cys. (c) Cou-Hcy. (d) Cou-GSH.

The total DOS (TDOS) of the probe and sensing product molecules and the partial DOS of two individual parts in the molecules (coumarin part and benzene ring in the probe and biothiols in the sensing product) are all depicted within Figure 7. It could be seen that the obvious charge transfer characteristic in the electron excitation process between  $S_0$  and  $S_1$  in the CouSeNO<sub>2</sub> probe, in which the HOMO was mainly contributed by the benzene ring part and the LUMO was mainly contributed by the coumarin part. This charge transfer character indicated that the ICT process led to the small oscillation strength between the  $S_0$  and  $S_1$  states and a weak fluorescent intensity in the original CouSeNO<sub>2</sub> probe. Otherwise, the local excitation characteristic was shown in the electron excitation process between  $S_0$  and  $S_1$  in the sensing products through the probe reaction with the biothiols, which led to the corresponding significant oscillation strength and fluorescent intensity. Due to the different molecular structures of the biothiols, the sensing product Cou-GSH without its 7–8-membered rings showed a wavelength red shift in maximum absorption peak and fluorescence compared with the original CouSeNO<sub>2</sub> probe. Contrarily, the Michael addition reaction between the thiol groups (Cys and Hcy) and the unsaturated C=C double bond in the CouSeNO<sub>2</sub> probe led to the formation of the 7–8-membered rings in the sensing products Cou-Cys and Cou-Hcy, which made the different electronic structure variation compared with the original probe CouSeNO<sub>2</sub>. Both the wavelength of the maximum absorption peak and fluorescence took a blue shift relative to the CouSeNO<sub>2</sub> probe. The blue and red absorption shifts of CouSeNO<sub>2</sub> with Cys, Hcy, and GSH were clearly related to the HOMO/LUMO energy gaps of the corresponding sensing products.

So, the different wavelengths and colors of the fluorescence from the sensing product with the biothiols (Cys, Hcy, and GSH) allowed for the CouSeNO<sub>2</sub> probe to be successfully applied in distinguishing the detection of the small-molecule biothiols.

### 3. Theoretical Methods

The theoretical methods of the research for the fluorescent probe CouSeNO<sub>2</sub>/CouSNO<sub>2</sub> sensing biothiols were as follows:

1. The functional and basis set combination CAM-B3LYP/def2-TZVPD was used in structure optimization, corresponding vibrational frequency analysis on the probe, and sensing product conformations with ORCA program 5.1 [30–33]. Non-imaginary frequency was found in the vibrational analysis on the stable geometric structure, which confirmed the stability of the structure optimization results. The wB2GP-PLYP/def2-TZVPD combination was used in single-point energy to obtain free energy with high precision, according to benchmark research [34]. Similar calculated results were obtained in the gas phase and in several solvents with different polarities, which indicated that this fluorescent probe was insensitive to the solvent effect.
2. The electronic structure and fluorescent properties of the probe and its sensing products were obtained through the Multiwfn 3.8(dev) code [35] based on the DFT and TDDFT results through the ORCA program.
3. The reorganization energy and Huang–Rhys factors between the S<sub>0</sub> and S<sub>1</sub> states of the probe and sensing products were obtained through the Dushin program.
4. Most of the figures in this work were rendered by means of VMD 1.9.3 software [36].

### 4. Conclusions

The electron structure and fluorescent theoretical analysis indicated a local excitation character for the electron excitation process from S<sub>0</sub> to S<sub>1</sub> within the sensing product of the CouSeNO<sub>2</sub> probe's reaction with small-molecule biothiols, including Cys/Hcy and GSH. Due to the different molecular structures of the biothiols, the sensing product Cou-GSH without its 7–8-membered rings showed a wavelength red shift in its maximum absorption peak and fluorescence compared with the original CouSeNO<sub>2</sub> probe. Contrarily, the Michael addition reaction between the thiol groups (Cys and Hcy) and the unsaturated C=C double bond in the CouSeNO<sub>2</sub> probe led to both the wavelengths of the maximum absorption peak and fluorescence taking a blue shift relative to the CouSeNO<sub>2</sub> probe. So, the different wavelengths and colors of the fluorescence from the sensing product with the biothiols (Cys, Hcy, and GSH) allowed for the CouSeNO<sub>2</sub> probe to be successfully applied in distinguishing the detection of the exogenous and endogenous biothiols in living cells. The theoretical investigation of the mechanism of fluorescent probe molecular design would provide insights into building highly efficient fluorescent probes for biothiol detection in the future.

**Funding:** This research was funded by Natural Science Foundation of Liaoning Province (2022-MS-389, 20180550512, JYTQN201923).

**Institutional Review Board Statement:** Not applicable.

**Informed Consent Statement:** Not applicable.

**Data Availability Statement:** The data presented in this study are available in article.

**Conflicts of Interest:** The authors declare no conflict of interest.

### References

1. Han, H.; Wang, F.; Chen, J.; Li, X.; Fu, G.; Zhou, J.; Zhou, D.; Wu, W.; Chen, H. Changes in Biothiol Levels Are Closely Associated with Alzheimer's Disease. *J. Alzheimers Dis.* **2021**, *82*, 527–540. [PubMed]
2. Campodonico, P.R.; Alarcon-Esposito, J.; Olivares, B. Kinetics and Reaction Mechanism of Biothiols Involved in S<sub>N</sub>Ar Reactions: An Experimental Study. *Front. Chem.* **2022**, *10*, 142214.

3. Hu, Y.; Zeng, F. A theranostic prodrug based on FRET for real-time drug release monitoring in response to biothiols. *Mater. Sci. Eng. C-Mater. Biol. Appl.* **2017**, *72*, 77–85. [[PubMed](#)]
4. Si, L.; Fu, Q.; Shi, Z.; Zhang, T.; Hou, Q.; Xu, Z.; Ai, S. The fluorescent detection of biothiols and antimicrobial study based on copper(I) iodide coordination polymer. *Dye. Pigment.* **2023**, *215*, 2134–2146.
5. Nagendraraj, T.; Priya, S.V.; Annaraj, J.; Sagadevan, S. Targeted cysteine and glutathione detection in extra/intracellular systems by copper-based fluorescent imaging probes. *Coord. Chem. Rev.* **2023**, *495*, 1089–1101.
6. Ma, C.; Yan, D.; Hou, P.; Liu, X.; Wang, H.; Xia, C.; Li, G.; Chen, S. Bioimaging and Sensing Thiols In Vivo and in Tumor Tissues Based on a Near-Infrared Fluorescent Probe with Large Stokes Shift. *Molecules* **2023**, *28*, 5702. [[PubMed](#)]
7. Feng, Q.; Song, Y.; Ma, Y.; Deng, Y.; Xu, P.; Sheng, K.; Zhang, Y.; Li, J.; Wu, S. Molecular engineering of benzenesulfonyl analogs for visual hydrogen polysulfide fluorescent probes based on Nile red skeleton. *Spectrochim. Acta Part A-Mol. Biomol. Spectrosc.* **2023**, *296*, 135466.
8. Sun, Y.; Wang, Y.; Lu, Y.; Kong, X.; Wei, H.; Chen, Q.; Yan, M.; Dong, B. Mitochondria-targeted and FRET-based fluorescent probe for the imaging of endogenous SO<sub>2</sub> in living cells. *Spectrochim. Acta Part A-Mol. Biomol. Spectrosc.* **2022**, *265*, 110233. [[CrossRef](#)]
9. Bhasin, A.K.K.; Chauhan, P.; Chaudhary, S.; Umar, A.; Baskoutas, S. Highly Sensitive and Selective Sulfite Ion Sensor Based on Biochemically Stable Iodo-Functionalized Coumarin Fluorophores. *Chemistryselect* **2022**, *7*, 224361. [[CrossRef](#)]
10. Zhu, Y.; Pan, H.; Song, Y.; Jing, C.; Gan, J.-A.; Zhang, J. Mitochondria-targeted fluorescent probe for rapid detection of thiols and its application in bioimaging. *Dye. Pigment.* **2021**, *191*, 3647–3658.
11. Li, H.; An, Y.; Gao, J.; Yang, M.; Luo, J.; Li, X.; Lv, J.; Li, X.; Yuan, Z.; Ma, H. Recent Advances of Fluorescence Probes for Imaging of Ferroptosis Process. *Chemosensors* **2022**, *10*, 233. [[CrossRef](#)]
12. Khan, Z.G.; Patil, M.R.; Nangare, S.N.; Patil, A.G.; Boddu, S.H.S.; Tade, R.S.; Patil, P.O. Surface nanoarchitected metal-organic frameworks-based sensor for reduced glutathione sensing: A review. *J. Nanostruct. Chem.* **2022**, *12*, 1053–1074.
13. Yang, Q.; Lan, T.; He, W. Recent progress in reaction-based fluorescent probes for active sulfur small molecules. *Dye. Pigment.* **2021**, *186*, 3145–3156. [[CrossRef](#)]
14. Su, S.; Chen, Q.; Wang, C.; Jing, J.; Zhang, X. A Sensitive Fluorescent Probe for Homocysteine/Cysteine in Pure Aqueous Media and Mitochondria. *Chemistryselect* **2021**, *6*, 8391–8396. [[CrossRef](#)]
15. Raut, J.; Sahoo, P. Detection of Biothiols Using Some Novel Chemosensors: An Overview. *Mini Rev. Org. Chem.* **2021**, *18*, 867–884. [[CrossRef](#)]
16. Liu, W.; Chen, J.; Xu, Z. Fluorescent probes for biothiols based on metal complex. *Coord. Chem. Rev.* **2021**, *429*, 241756.
17. Xue, L.; Yu, D.; Sun, J.; Guan, L.; Xie, C.; Wang, L.; Jia, Y.; Tian, J.; Fan, H.; Sun, H. Rapid GSH detection and versatile peptide/protein labelling to track cell penetration using coumarin-based probes. *Analyst* **2023**, *148*, 532–538. [[CrossRef](#)]
18. Jiang, H.; Yin, G.; Gan, Y.; Yu, T.; Zhang, Y.; Li, H.; Yin, P. A multisite-binding fluorescent probe for simultaneous monitoring of mitochondrial homocysteine, cysteine and glutathione in live cells and zebrafish. *Chin. Chem. Lett.* **2022**, *33*, 1609–1612. [[CrossRef](#)]
19. Hao, Y.; Zhang, Y.; Luo, L.; Zhu, D.; Xu, M.; Zeng, R.; Chen, S. Deep-Red Emissive Fluorescent Probe for Sensitive Detection of Cysteine in Milk and Living Cells. *Food Anal. Methods* **2022**, *15*, 2145–2154. [[CrossRef](#)]
20. Zhang, Y.; Xu, C.; Sun, H.; Ren, M.; Kong, F. A Cys-regulated fluorescent probe targeting cancer cells and their application in inflammation detection. *J. Photochem. Photobiol. A-Chem.* **2023**, *444*, 7241–7253. [[CrossRef](#)]
21. Wang, Z.; Li, X.; Sun, X.; Zhang, X.; He, C.; Li, Y.; Lu, F.; Lu, X.; Fan, Q. Highly selective imaging of intratumoral hydrogen sulfide by NIR-II emissive fluorescent probes. *Sens. Actuators B-Chem.* **2023**, *384*, 6325–6337. [[CrossRef](#)]
22. Chen, X.G.; Mei, Y.; Song, Q.H. A 3-(2'-nitro vinyl)-4-phenylselenyl coumarin as a fluorescent probe for distinguishing detection of Cys/Hcy and GSH. *Dye. Pigment.* **2022**, *203*, 11032. [[CrossRef](#)]
23. Kohut, S.V.; Cuevas-Saavedra, R.; Staroverov, V.N. Generalized average local ionization energy and its representations in terms of Dyson and energy orbitals. *J. Chem. Phys.* **2016**, *145*, 2568–2574. [[CrossRef](#)] [[PubMed](#)]
24. Zamora, P.P.; Bieger, K.; Cuchillo, A.; Tello, A.; Muena, J.P. Theoretical determination of a reaction intermediate: Fukui function analysis, dual reactivity descriptor and activation energy. *J. Mol. Struct.* **2021**, *1227*, 129369. [[CrossRef](#)]
25. Sanchez-Marquez, J. New advances in conceptual-DFT: An alternative way to calculate the Fukui function and dual descriptor. *J. Mol. Model.* **2019**, *25*, 5214–5226. [[CrossRef](#)]
26. Martinez-Araya, J.I. Why is the dual descriptor a more accurate local reactivity descriptor than Fukui functions? *J. Math. Chem.* **2015**, *53*, 451–465. [[CrossRef](#)]
27. Wei, Y.-C.; Hsu, L.-Y. Polaritonic Huang-Rhys Factor: Basic Concepts and Quantifying Light-Matter Interactions in Media. *J. Phys. Chem. Lett.* **2023**, *14*, 2395–2401. [[CrossRef](#)]
28. Filipowska, K.; Pawlikowski, M.T.; Andrzejak, M. Optical Spectra of Oligofurans: A Theoretical Approach to the Transition Energies, Reorganization Energies, and the Vibronic Activity. *Molecules* **2021**, *26*, 7458. [[CrossRef](#)]
29. Reimers, J.R. A practical method for the use of curvilinear coordinates in calculations of normal-mode-projected displacements and Duschinsky rotation matrices for large molecules. *J. Chem. Phys.* **2001**, *115*, 9103–9109. [[CrossRef](#)]
30. Neese, F. Software update: The ORCA program system-Version 5.0. *Wiley Interdiscip. Rev.-Comput. Mol. Sci.* **2022**, *12*, 3251–3264. [[CrossRef](#)]
31. Liu, P.; Liu, Y.L.; Huang, H.; Bai, G.; Peng, Y.J. Theoretical investigation on FRET strategy of ratio metric fluorescent probe sensing hydrogen sulfide. *Spectrochim. Acta Part A-Mol. Biomol. Spectrosc.* **2023**, *289*, 122223. [[CrossRef](#)] [[PubMed](#)]

32. Liu, Y.-L.; Huang, H.; Peng, Y.-J. Fluorescent probe for simultaneous detection of human serum albumin and sulfite: A theoretical analysis. *J. Mol. Struct.* **2022**, *1255*, 132441. [[CrossRef](#)]
33. Fu, L.; Huang, H.; Zuo, Z.; Peng, Y. A Single Organic Fluorescent Probe for the Discrimination of Dual Spontaneous ROS in Living Organisms: Theoretical Approach. *Molecules* **2023**, *28*, 6983. [[CrossRef](#)] [[PubMed](#)]
34. Casanova-Páez, M.; Dardis, M.B.; Goerigk, L.  $\omega$ B2PLYP and  $\omega$ B2GPPLYP: The First Two Double-Hybrid Density Functionals with Long-Range Correction Optimized for Excitation Energies. *J. Chem. Theory Comput.* **2019**, *15*, 4735–4744. [[CrossRef](#)]
35. Lu, T.; Chen, F. Multiwfn: A multifunctional wavefunction analyzer. *J. Comput. Chem.* **2012**, *33*, 580–592. [[CrossRef](#)]
36. Humphrey, W.; Dalke, A.; Schulten, K.K. VMD—Visual molecular dynamics. *J. Mol. Graph.* **1995**, *14*, 33–38. [[CrossRef](#)]

**Disclaimer/Publisher’s Note:** The statements, opinions and data contained in all publications are solely those of the individual author(s) and contributor(s) and not of MDPI and/or the editor(s). MDPI and/or the editor(s) disclaim responsibility for any injury to people or property resulting from any ideas, methods, instructions or products referred to in the content.